# SANDIA REPORT

SAND2020-6744x
Printed June 2020

Sandia National Laboratories

# Computational Model for Microballistic Perforation of Multilayer Graphene

Stewart A. Silling
Müge Fermen-Coker

Prepared by
Sandia National Laboratories
Albuquerque, New Mexico 87185
Livermore, California 94550

Issued by Sandia National Laboratories, operated for the United States Department of Energy by National Technology & Engineering Solutions of Sandia, LLC.



Available to DOE and DOE contractors from

U.S. Department of Energy
Office of Scientific and Technical Information
P.O. Box 62
Oak Ridge, TN 37831

Telephone: (865) 576-8401
Facsimile: (865) 576-5728
E-Mail: reports@osti.gov
Online ordering: http://www.osti.gov/scitech

Available to the public from

U.S. Department of Commerce
National Technical Information Service
5301 Shawnee Road
Alexandria, VA 22312

Telephone: (800) 553-6847
Facsimile: (703) 605-6900
E-Mail: orders@ntis.gov
Online order: https://classic.ntis.gov/help/order-methods

# ABSTRACT

The peridynamic theory of solid mechanics is applied to the continuum modeling of the impact of small, high-velocity silica spheres on multilayer graphene targets. The model treats the laminate as a brittle elastic membrane. The material model includes separate failure criteria for the initial rupture of the membrane and for propagating cracks. Material variability is incorporated by assigning random variations in elastic properties within Voronoi cells. The computational model is shown to reproduce the primary aspects of the response observed in experiments, including the growth of a family of radial cracks from the point of impact.

# ACKNOWLEDGMENT

This work was supported by the U.S. Army Research Laboratory and by the DoD/DOE Joint Munitions Program at Sandia National Laboratories. Helpful discussions with Professor J.-H. Lee are gratefully acknowledged.

# CONTENTS



# LIST OF FIGURES

# 1. INTRODUCTION

Numerous experimental and theoretical studies have found that single layer graphene sheets have high elastic modulus and tensile strength [2, 1, 3]. Possible applications of graphene in engineering may require multilayer laminates, rather than single sheets, yet relatively little is known about the mechanical properties of multilayer graphene. In this paper, a continuum computational model is developed for multilayer graphene and compared with the microballistic data of Lee et al. [4]. In these microballistic experiments, a projectile with diameter $3.7\mu$m is launched against a multilayer target with velocities up to 900m-s$^{-1}$. The measured residual velocity, together with post-test imaging of the targets, provides information about the failure properties of multilayer graphene. The computational model uses the peridynamic theory of solid mechanics, which is a generalization of the standard theory that is more compatible with the direct simulation of growing cracks. The peridynamic theory, together with a new material model that is application to graphene laminates, is described in the next Section.

# 2. PERIDYNAMIC CONTINUUM MODEL

The peridynamic theory is a nonlocal generalization of the classical theory of solid mechanics that uses integro-differential equations, rather than partial differential equations. The peridynamic equations do not require the evaluation of the spatial derivatives of the deformation and are therefore more compatible with the direct simulation of discontinuities such as growing cracks. In the peridynamic theory, each material point $\mathbf{x}$ interacts through a material model with its neighbors within a cutoff distance in the refence configuration called the *horizon*, denoted by $\delta$. The material within the horizon of $\mathbf{x}$ is called the *family* of $\mathbf{x}$, denoted by $\mathscr{H}_{\mathbf{x}}$. The linear momentum balance has the following form:

$$\rho(\mathbf{x})\ddot{\mathbf{y}}(\mathbf{x},t) = \int_{\mathscr{H}_{\mathbf{x}}} \mathbf{f}(\mathbf{q},\mathbf{x},t)\, \mathrm{d}V_{\mathbf{q}} + \mathbf{b}(\mathbf{x},t) \tag{1}$$

where $\rho$ is the mass density, $\mathbf{y}$ is the deformation map, and $\mathbf{b}$ is the external body force density. The vector $\mathbf{f}(\mathbf{q},\mathbf{x},t)$ represents the *pairwise force density* (with units of force/volume$^2$) in the *bond* from $\mathbf{x}$ to $\mathbf{q}$. The integral in (1) sums up these interactions and can be thought of as a continuous version of molecular dynamics.

The pairwise force density is determined by the material model for the current deformation of $\mathscr{H}_{\mathbf{x}}$. The anti-symmetry condition given by

$$\mathbf{f}(\mathbf{x},\mathbf{q},t) = -\mathbf{f}(\mathbf{q},\mathbf{x},t) \tag{2}$$

is required for all material models, as a consequence of Newton's third law.

The simplest peridynamic material model is called *linear microelastic*. This model treats each bond as a linear spring. Let $\boldsymbol{\xi}$ denote the bond from $\mathbf{x}$ to $\mathbf{q}$:

$$\boldsymbol{\xi} = \mathbf{q} - \mathbf{x}. \tag{3}$$

At any time $t$, the *bond strain* in $\mathbf{x}$ is given by the change in length divided by its initial length:

$$s(\boldsymbol{\xi},t) = \frac{|\mathbf{y}(\mathbf{q},t) - \mathbf{y}(\mathbf{x},t)|}{|\mathbf{q}-\mathbf{x}|} - 1. \tag{4}$$

In the linear microelastic material model, the pairwise bond force density is given by

$$\mathbf{f}(\mathbf{q},\mathbf{x},t) = cs(\boldsymbol{\xi},t)\mathbf{M}(\boldsymbol{\xi},t) \tag{5}$$

where $c$ is a constant that determines the elastic modulus and $\mathbf{M}$ is the unit vector in the direction of the deformed bond:

$$\mathbf{M}(\boldsymbol{\xi},t) = \frac{\mathbf{y}(\mathbf{q},t) - \mathbf{y}(\mathbf{x},t)}{|\mathbf{y}(\mathbf{q},t) - \mathbf{y}(\mathbf{x},t)|}. \tag{6}$$

The form of (5) implies that the pairwise bond force density is always parallel to the deformed bond. This ensures that each bond interaction satisfies the balance of angular, as well as linear, momentum.

To incorporate damage into this material model, it is assumed that each bond can *break* irreversibly, after which it no longer sustains any load. The expression (5) is modified as follows:

$$\mathbf{f}(\mathbf{q},\mathbf{x},t) = cs(\boldsymbol{\xi},t)\mathbf{M}(\boldsymbol{\xi},t)\mu(\mathbf{x},t) \tag{7}$$

where $\mu$ is a damage variable that has the value 1 for unbroken bonds and 0 for broken bonds. The evolution of $\mu$ is defined by a damage law. The *net damage* is a measure of how many bonds connected to $\mathbf{x}$ have been broken:

$$\phi(\mathbf{x},t) = 1 - \frac{\int_{\mathscr{H}_\mathbf{x}} \mu(\mathbf{x}',t)\, dV_{\mathbf{x}'}}{\int_{\mathscr{H}_\mathbf{x}} dV_{\mathbf{x}'}} \tag{8}$$

It is also helpful to define the maximum damage in the family of $\mathbf{x}$ at any time:

$$\bar{\phi}(\mathbf{x},t) = \max_{\mathbf{x}'\in\mathscr{H}_\mathbf{x}} \phi(\mathbf{x}',t). \tag{9}$$

The simplest damage law causes a bond to break when its strain exceeds a critical value $s_0$:

$$\mu(\boldsymbol{\xi},0) = 1, \qquad \dot{\mu}(\boldsymbol{\xi},t) = -\Delta(t - t_{break}) \tag{10}$$

where $\Delta$ is the Dirac delta function and $t_{break}$ is the first time at which $s(\xi,t) \geq s_0$. $s_0$ is called the *critical strain* for bond breakage.

If the critical strain is a constant, the resulting material model is called the *prototype microelastic brittle* (PMB) material [6]. In the PMB material, $s_0$ can be determined according to the critical energy release rate for a material, which can be measured by laboratory testing. Conceptually, this provides the basic connection between peridynamics and classical linear elastic fracture mechanics.

The key advantage of the peridynamic method for simulating fracture is that cracks nucleate and grow autonomously according the conditions at each bond. There is no need to explicitly evaluate quantities such as the stress intensity factor, which are important in classical fracture mechanics. When each bond breaks, the load it was carrying tends to be transferred to other unbroken bonds, making it more likely that they will break. This leads to a continuing process of progressive failure. In practice, these failures occur along surfaces that represent cracks.

A limitation of the PMB material model is that the single constant $s_0$ determines both the nucleation and growth phases of fracture. For most real materials, this is not justified, because the concept of energy release rate only applies when a crack is already present. In the present application to graphene, this limitation causes unacceptable disagreement with the experimental data on microballistic impact. However, a large improvement is obtained by assuming that $s_0$ takes on either of two different values depending on whether the material in the family of $\mathbf{x}$ is damaged or undamaged:

$$s_0(\mathbf{x},t) = \begin{cases} s_{nuc}, & \text{if } \bar{\phi}(\mathbf{x},t) < \bar{\phi}_{trans} \\ s_{growth}, & \text{otherwise} \end{cases} \tag{11}$$

where $s_{nuc}$ and $s_{growth}$ are constants and $\bar{\phi}_{trans}$ is a constant that determines the damage at which the transition from nucleation to growth occurs. The general idea is that $s_{nuc}$ determines the strain at which failure first occurs, while $s_{growth}$ determines the energy release rate for cracks that have already been formed. The peridynamic material model specified by equations (7)-(11) is called the *microelastic nucleation and growth* (MNG) model.

Although the MNG model involves a transition from one value of $s_0$ to another, this does not adversely affect the autonomous nature of crack growth in the peridynamic theory. A point $\mathbf{x}$ that is within a distance $\delta$ of an existing crack changes from the nucleation value of critical bond strain to the growth value. This change happens independently among all the material points in the body.

# 3. MICROBALLISTIC TESTING

Lee *et al.* performed microballistic experiments on multilayer graphene sheets [4]. In these experiments, a silica sphere with diameter $3.7\mu$m was launched toward a graphene target that was supported at the edges. The nominal impact velocities were either 600m-s$^{-1}$ or 900m-s$^{-1}$. The target thicknesses varied between $0.02\mu$m and $0.10\mu$m. In addition to the initial (launch) velocity of the projectile, the residual velocity after perforation of the target was measured. The resulting change in kinetic energy, after accounting for air resistance, was reported.

Typically in these experiments, the projectile after perforation is essentially undamaged and can be treated as a rigid body. Because of the high tensile strength of the graphene, it sustains large deflections and membrane strains near the point of impact. This creates a propagating deflection that moves away from the point of impact and has a conical shape that grows linearly in time in both diameter and height. The membrane strains within this graphene cone store strain energy. After rupture first occurs near the point of impact, this strain energy provides the driving force for the rapid growth of a family of radial cracks. These cracks propagate until they have dissipated so much of the strain energy that there is no longer a sufficient driving force to make them grow further, and they arrest. The material between the radial cracks forms petals that are observed in post-test SEM images to fold behind the initial plane of the target.

A schematic diagram (not to scale) of the microballistic impact experiment is shown in Figure 3-1, along with a typical SEM image of the post-test target.

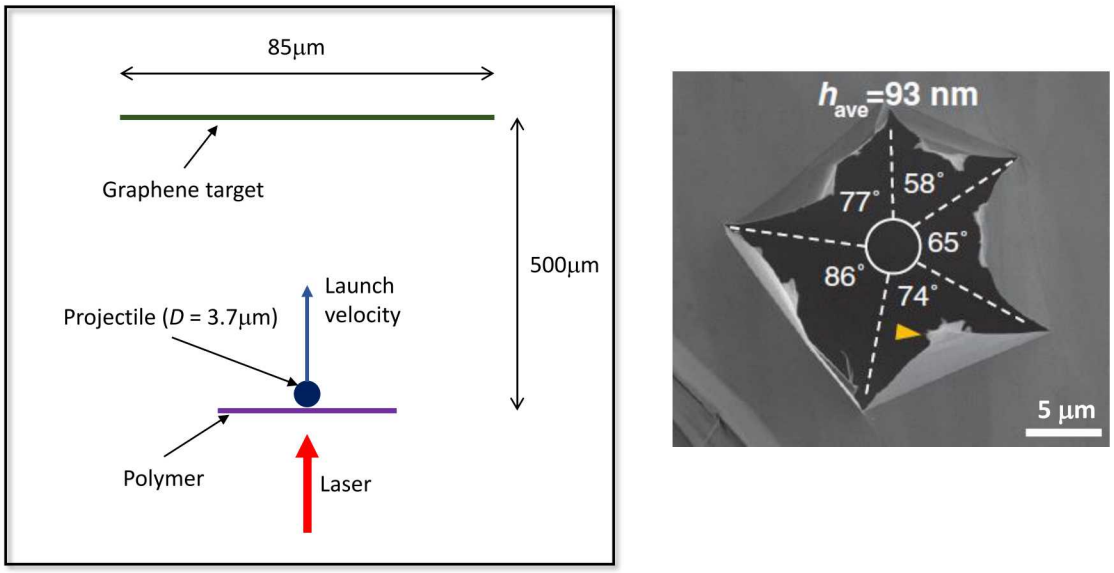


**Figure 3-1 Left: schematic diagram of the microballistic impact experiment. Right: SEM image of a typical post-test target [4].**

# 4. MODEL FOR MULTILAYER GRAPHENE

Because the multilayer graphene targets are much thinner than the projectile diameter, it is valid to assume that the bending resistance in the target is a negligible effect. Therefore, the target is treated as a membrane. The material model for multilayer graphene is the MNG described in Section 1.

It was found experimentally that the thickness of the graphene targets varied spatially with a coefficient of variation (CV) of about 20%. This variation apparently is one cause of the variability in results among different shots with nominally the same target and impact conditions. The spatial variability of the thickness was accounted for in the peridynamic model by assigning randomly generated Voronoi cells to each point in the membrane. Each cell was assigned a random number $r \in [0,1]$ drawn from a uniform distribution. The elastic constant $c$ in the material model (5) was then varied accordingly by incorporating a random term into (5):

$$\mathbf{f}(\mathbf{q},\mathbf{x},t) = c(r)s(\boldsymbol{\xi},t)\mathbf{M}(\boldsymbol{\xi},t), \qquad c(r) = c_0 Q(r) \tag{12}$$

where $c_0$ is the nominal (mean) bond elastic constant and $Q$ is defined by

$$Q(r) = 1 + \frac{2\Delta Q}{\pi}\sin^{-1}(2r-1) \tag{13}$$

where $\Delta Q$ is a constant between 0 and 1, and $\sin^{-1}(\cdot) \in [-\pi/2, \pi/2]$. The resulting probability distribution for $s_0$ is shown in Figure 4-1. A typical Voronoi cell structure is shown in Figure 4-2, along with the projectile.

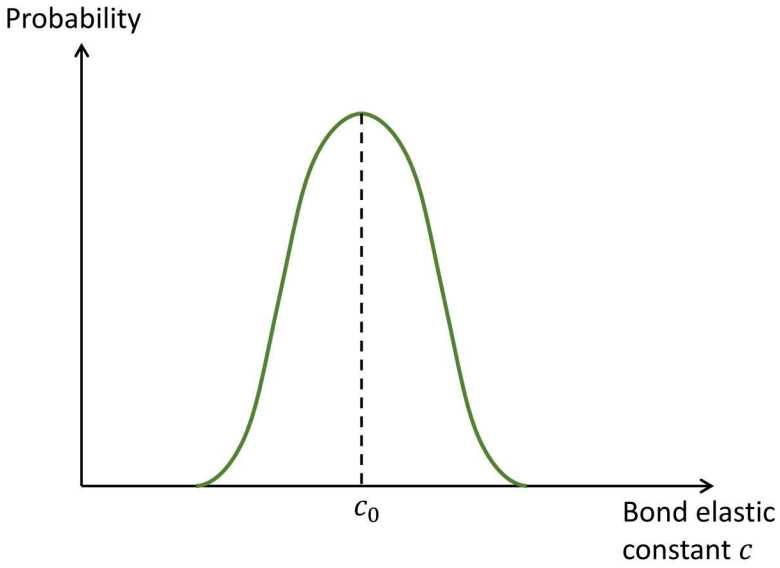


**Figure 4-1 Probability distribution of values of the bond elastic constant $c$ assigned to different Voronoi cells.**

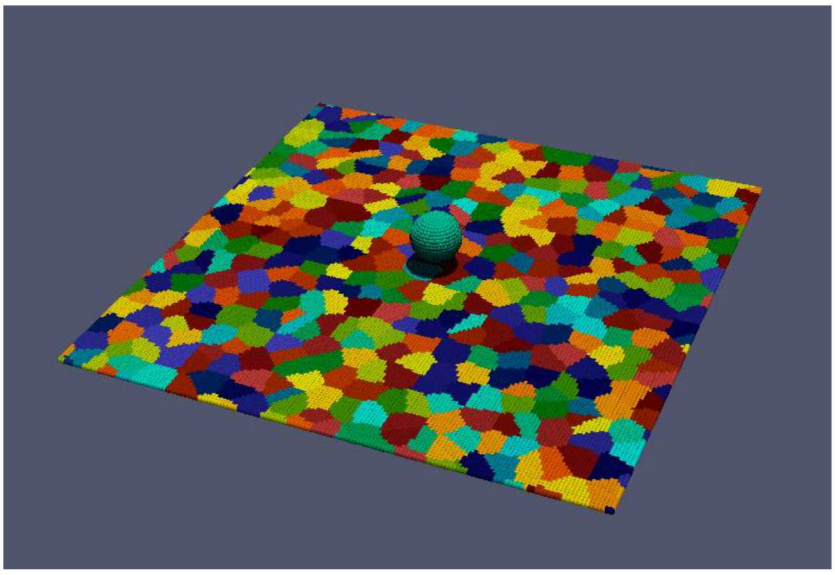

**Figure 4-2 Voronoi cells that are used to assign random variations in elastic properties to account for variations in thickness.**

# 5. SIMULATION RESULTS

A set of 40 peridynamic calculations was run for all possible combinations of the following parameters:

- Nominal target thickness (nm) = $\{20, 40, 60, 80, 100\}$.
- Launch velocity (m-s$^{-1}$) = $\{600, 900\}$.
- Voronoi random seed = $\{0, 1, 2, 3\}$.

The simulation code was Emu, which uses a meshless Lagrangian discretization with explicit time integration [6]. In all cases, the grid had about 28,000 nodes and a grid spacing of 0.25$\mu$m. The bond elastic constant $c_0$ was calibrated to reproduce a wave speed of 16,000m-s$^{-1}$. The mass density of the graphene in the model was 2200kg-m$^{-3}$. The calculations were run out to a time of 60ns, by which time the crack propagation and folding of petals had essentially stopped. The following additional parameters were used: $s_{nuc} = 0.35$, $s_{growth} = 0.04$, $\delta = 0.775\mu$m, $\bar{\phi}_{trans} = 0.2$. The nominal spacing of the Voronoi cells was 2.0$\mu$m, and the variability coefficient was $\Delta Q = 0.4$.

The impact velocity of the projectile in the simulations was reduced below the launch velocity to account for energy loss due to air resistance, which was estimated to be $\Delta E_{air} = 1.09$nJ [4]. The projectile and graphene target interacted through contact forces [5]. These forces cause nodes in different materials to repel when they approach each other within a predefined distance on the order of the grid spacing. The forces were sufficiently large to avoid interpenetration of materials. Friction and drag forces at the contact surfaces were also investigated but found not to improve the agreement with the test data, and so were not pursued further.

Typical model results after perforation are shown in Figure 5-1. The case on the left, resulting in four petals, has a graphene thickness of 80nm and a launch velocity of 600m-s$^{-1}$. In the case shown on the right, the graphene thickness is 60nm and the launch velocity is 600m-s$^{-1}$. This combination of conditions, together with this particular Voronoi cell structure, results in five petals.

As an aid to the systematic interpretation of the 40 calculations, an algorithm was developed to count the number of petals in a model. This algorithm works by first identifying the crack tip positions (Figure 5-2). This is done by searching for isolated high-strain locations in the deformed grid. These points, when connected by line segments after sorting according to angle in the plane, form a polygon. However, the number of these vertices or line segments can be greater than the number of petals, because some petals contain smaller arrested cracks. Therefore, the convex hull of this polygon is constructed to omit these smaller cracks. The number of vertices or sides of this convex hull is the number of petals according to this algorithm. The distribution of the number of petals in the 50 cases are shown in Figure 5-3. This distribution is similar the one found from a large number of experiments reported in [4].

Figure 5-4 shows the computed (red) and measured (blue) values for kinetic energy lost by the projectile due to air resistance and impact on the graphene. The energy lost due to air resistance is

estimated [4] to be $\Delta E_{air} \approx 1.09nJ$. This can be computed from the stagnation pressure of the projectile in air. The values plotted in Figure 5-4 are given by

$$\Delta E = \frac{m}{2}(V_{launch}^2 - V_{exit}^2) \tag{14}$$

where $m$ is the mass of the projectile (0.0504ng), and $V_{launch}$ and $V_{exit}$ are the projectile velocities at launch and exit (after perforation of the target) respectively.

Figure 5-5 shows the computed (red) and measured (blue) values for maximum radial crack length. This is the maximum length among all the radial cracks in a given impact.

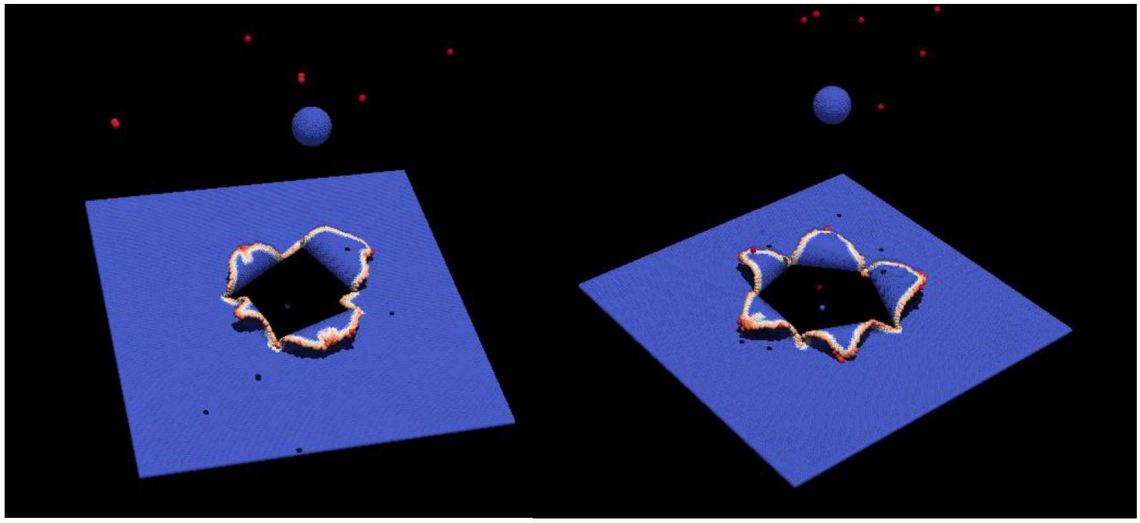

**Figure 5-1 Typical models of a target after perforation.**

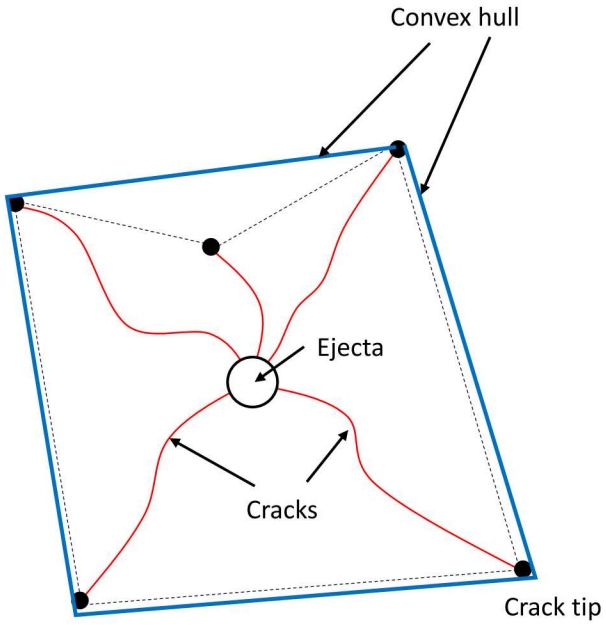


**Figure 5-2 Petal counting algorithm. The number of petals equals the number of sides of the convex hull of the polygon whose vertices are the crack tips.**

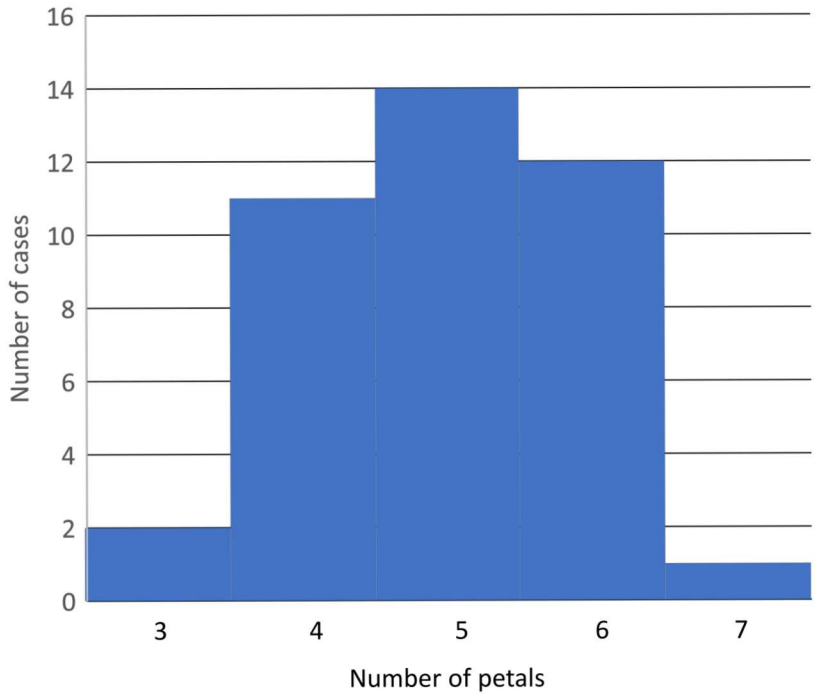


**Figure 5-3 Histogram of the number of petals in the 40 cases.**

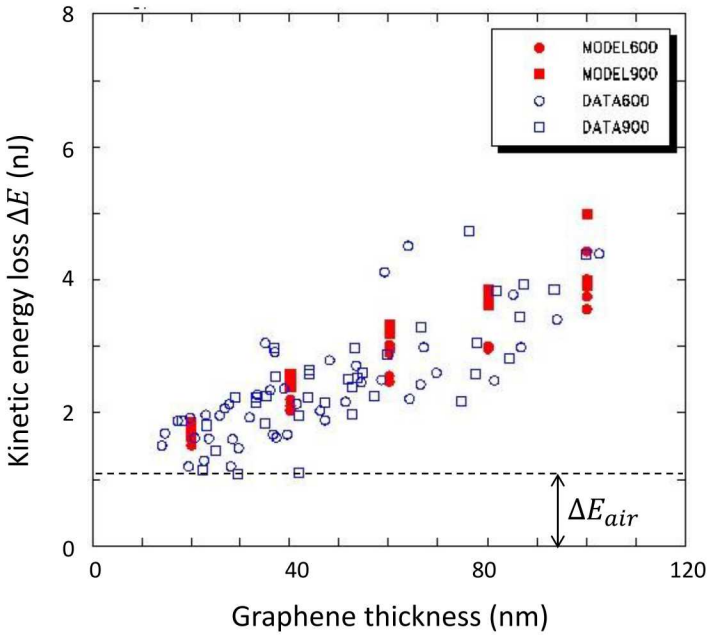


**Figure 5-4 Projectile kinetic energy change due to impact.**

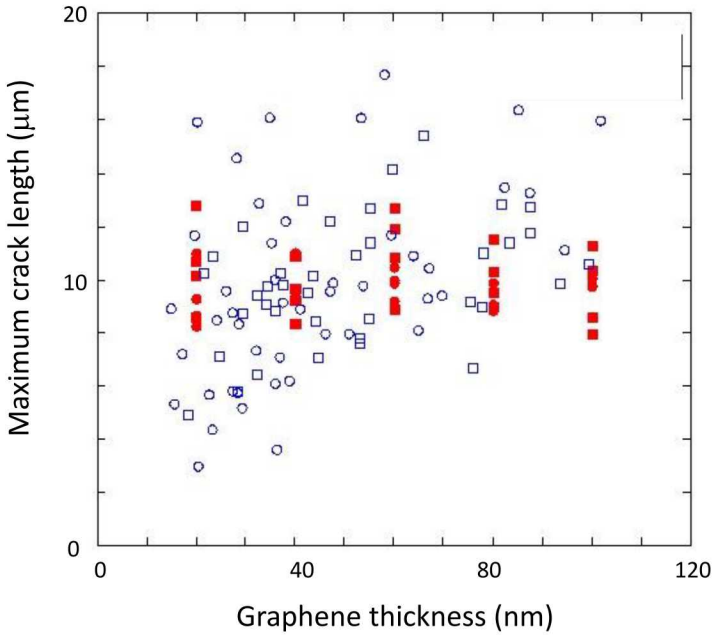


**Figure 5-5 Maximum radial crack length from the point of impact.**

# 6. DISCUSSION

The results in this paper demonstrate the applicability of the peridynamic continuum model to simulating the perforation of brittle elastic membranes. The use of separate rupture (nucleation) and growth parameters for cracks in the new MNG material model allows both the residual projectile energy and the general features of cracking and petalling to be reproduced. The MNG model adds two additional parameters to the widely-used PMB material model.

The number of radial cracks or petals is determined primarily by the availability of strain energy at the time when rupture first occurs at or near the point of impact. The time of this rupture, and therefore the available strain energy, are influenced not only by the nucleation bond strain $s_{nuc}$, but also by the elastic constant $c(r)$ at in the Voronoi cell at the point of impact. Lower values of $c(r)$ would lead to shorter and fewer radial cracks.

It is possible to define direction-dependent critical strains for bond failure as a type of anisotropic damage evolution law. Composite materials are generally modeled in this way in peridynamics [7]. However, in the present application, it was found that direction-dependent damage in the peridynamic model did not improve the agreement with the microballistic experimental data.

# REFERENCES


[1] C. Gómez-Navarro, M. Burghard, and K. Kern. Elastic properties of chemically derived single graphene sheets. *Nano letters*, 8:2045–2049, 2008.

[2] C. Lee, X. Wei, J. W. Kysar, and J. Hone. Measurement of the elastic properties and intrinsic strength of monolayer graphene. *science*, 321(5887):385–388, 2008.

[3] C. Lee, X. Wei, Q. Li, R. Carpick, J. W. Kysar, and J. Hone. Elastic and frictional properties of graphene. *physica status solidi (b)*, 246:2562–2567, 2009.

[4] J.-H. Lee, P. E. Loya, J. Lou, and E. L. Thomas. Dynamic mechanical behavior of multilayer graphene via supersonic projectile penetration. *Science*, 346:1092–1096, 2014.

[5] R. W. Macek and S. A. Silling. Peridynamics via finite element analysis. *Finite Elements in Analysis and Design*, 43:1169–1178, 2007.

[6] S. A. Silling and E. Askari. A meshfree method based on the peridynamic model of solid mechanics. *Computers and Structures*, 83:1526–1535, 2005.

[7] J. Xu, A. Askari, O. Weckner, and S. Silling. Peridynamic analysis of impact damage in composite laminates. *Journal of Aerospace Engineering*, 21:187–194, 2008.

# DISTRIBUTION

**Hardcopy—External**

| Number of Copies | Name(s) | Company Name and Company Mailing Address |
|---|---|---|
| | | |

**Hardcopy—Internal**

| Number of Copies | Name | Org. | Mailstop |
|---|---|---|---|
| | | | |

**Email—Internal** [redacted]

| Name | Org. | Sandia Email Address |
|---|---|---|
| Technical Library | 01177 | libref@sandia.gov |


Sandia National Laboratories is a multimission laboratory managed and operated by National Technology & Engineering Solutions of Sandia LLC, a wholly owned subsidiary of Honeywell International Inc., for the U.S. Department of Energy's National Nuclear Security Administration under contract DE-NA0003525.